SCANNING VOL. 28, 219-227 (2006)

Received: August 16, 2005
Accepted with revision: March 1, 2006

Parameters and Mechanisms Governing Image Contrast in Scanning Electron Microscopy of Single-Walled Carbon Nanotubes

W.K. WONG, A. NOJEH,* R.F.W. PEASE*

Department of Electrical and Computer Engineering, National University of Singapore, Singapore; *Department of Electrical Engineering, Stanford University, Stanford, California, USA

Summary: Image formation of single-walled carbon nanotubes (SWNTs) in the scanning electron microscope (SEM) is peculiarly sensitive to primary electron landing energy, imaging history, sample/substrate geometry, electrical conductivity, sample contamination, and substrate charging. This sensitivity is probably due to the extremely small interaction volume of the SWNTs' monolayered, nanoscale structures with the electron beam. Traditional electron beam/bulk specimen interaction models appear unable to explain the contrast behavior when directly applied to SWNTs. We present one systematic case study of SWNT SEM imaging with special attention to the above parameters and propose some physical explanations for the effect of each. We also demonstrate that it is possible to employ voltage biasing to counteract this extrinsic behavior, gain better control of the image contrast, and facilitate the interpretation of SWNT images in the SEM.

Key words: carbon nanotubes, scanning electron microscopy, electron beam specimen interaction, secondary electron emission, voltage contrast, electron beam-induced conductivity

PACS: 07.78.+s, 68.37.Hk, 41.75.Fr, 81.07.-b, 78.67.Ch

Introduction

The intrinsic advantages of the scanning electron microscope (SEM) such as high resolution (down to 1 nm in modern instruments), intuitive image interpretation, minimal sample preparation, high analysis throughput, and relatively low setup cost have led to the SEM being the present-day workhorse for high-resolution microanalysis. The past decade has seen SEM applications being expanded further to include that of nanodimensioned samples, with the catalyst being the discovery of the carbon nanotube (CNT) by Iijima (1991). The shank diameters of CNTs are in the range of 0.7–3 nm for single-walled CNTs (SWNTs) and higher (tens of nanometers) for multiwalled CNTs (MWNTs). This is close to the limit of resolution of the SEM; yet SWNTs are readily observable in the SEM, albeit with measured shank dimensions greater than both theoretical estimates and estimates obtained using other microanalytical tools. For example, Figure 1a shows diameters of a particular SWNT ranging from approximately 60 nm and 370 nm (estimated using full width at half maximum measurements from high-magnification SEM images of the SWNT) obtained by 2.0 keV SEM to 2.8 nm obtained by atomic force microscopy (AFM) (Fig. 1b). Also apparent from Figure 1a is the variable contrast behavior of the SWNTs, for example, comparing SWNTs over insulating versus conducting substrates. The image contrast of CNTs on insulators has previously been proposed to be based on potential differences between the CNT and the substrate (Brintlinger *et al*. 2002) and electron beam-induced current on the insulator surface (Homma *et al*. 2004). Here, we explore the issue further by investigating the role of primary electron landing energy and history of imaging, SWNT/substrate geometry, substrate conductivity, SWNT-substrate potential, and electron beam-deposited contamination. It will be shown that SWNT contrast does not always obey established bulk sample physics, but instead is strongly influenced by these extrinsic parameters due to the extremely limited interaction of the primary electron beam with the monolayer graphitic shell in a SWNT. This extrinsically determined contrast results in a high degree of variability in SEM analysis of nanostructures such as CNTs. It will be shown that specimen biasing can be employed in situ to tailor secondary electron (SE) emission from SWNTs to suit analysis objectives and negate some of the uncertainties presented by the above-mentioned factors.

Materials and Methods

Heterogeneous SWNT-dielectric-metallization devices have garnered much attention over the past few years (Martel *et al*. 1998, Radosavljevic *et al*. 2002); hence, a triode-type test

This study was funded by NSF under the NIRT program (ECS 0210899), DARPA Advanced Lithography Program and the U.S. Air Force under contract No. F33615-00-1-1728. This work was also supported in part by the Foundation for Advances in Medicine and Science, Inc. (FAMS).

Address for Reprints:

Dr. Wai Kin Wong
Department of Electrical and Computer Engineering
4 Engineering Drive 3
National University of Singapore
Singapore 119260

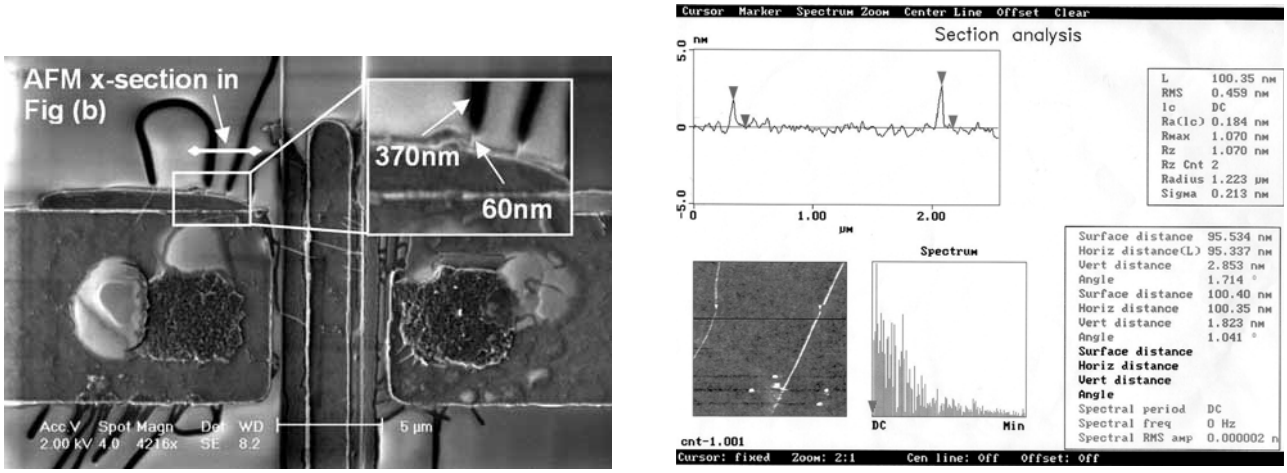

(a) (b)

FIG. 1 Shank diameter variations of a single-walled carbon nanotube observed using (a) Secondary electron imaging at 2.0 keV in an FEI Sirion scanning electron microscope (60 nm in the suspended region of the single-walled carbon nanotube, 370 nm for the region lying on silicon dioxide), horizontal field width = 29 µm; (b) contact mode atomic force microscopy (AFM) in a Digital Instruments Nanoscope AFM (2.8 nm).

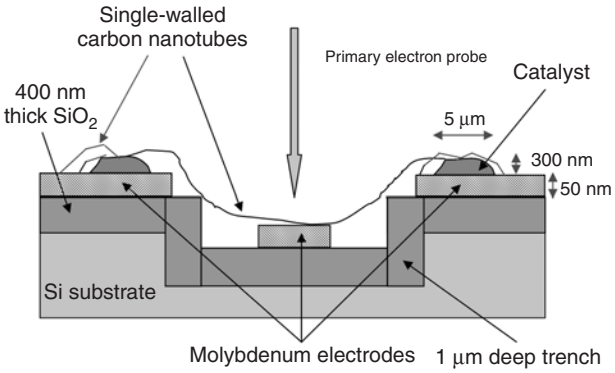

FIG. 2 Cross-sectional schematic of the test device (not to scale).

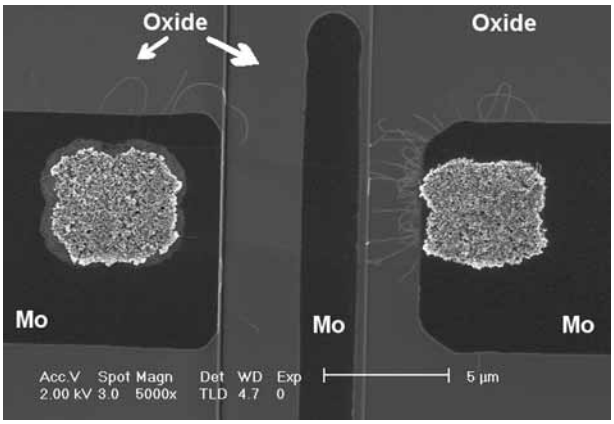

FIG. 3 2.0 keV scanning electron micrograph showing typical horizontally aligned single-walled carbon nanotube formation across the trench after thermal chemical vapor deposition growth (horizontal field width = 25 µm, FEI Sirion SEM).

structure was designed and fabricated (Fig. 2) to study the issues in the inspection of such devices in the SEM. The trenched design enabled the characterization of both suspended and nonsuspended SWNTs on dielectric and conducting regions. The trench was defined using optical lithography and dry etching. Thermal oxidation created the oxide layer, and optical lithography and lift-off were used to pattern the metal electrodes and SWNT growth catalyst islands that contain iron, molybdenum, and alumina. The SWNTs were grown via chemical vapor deposition (CVD) process using methane and ethylene precursors at 850–900°C. Hydrogen was used as a background gas during the CVD process. Total growth time was approximately 5 min. This process has been previously characterized to yield a very high percentage of horizontally oriented, single-walled CNTs (Cassell *et al.* 1999), with an example shown in Figure 3. Imaging was performed at vacuum chamber pressures of around 1×10^{-5} Torr on an FEI Sirion Schottky field emission SEM, as well as on a Hitachi S-2500 tungsten thermionic SEM at 5×10^{-5} Torr (Hitachi, Tokyo, Japan). For specimen biasing experiments, the test die was mounted in a 40-pin chip carrier, wire-bonded, and then placed into a custom SEM sample holder. Vacuum feedthroughs allowed in-situ electrical measurements and biasing to be performed in the Hitachi S-2500 SEM equipped with an in-lens detector, which allows more efficient and uniform SE collection at small working distances as the low energy secondaries are tightly collimated by the axial magnetic field of the objective lens (Fig. 4). This collection scheme also avoids shadowing effects prevalent with conventional SE detectors due to the axial symmetry of the SE extraction field of the objective lens.

The influence of the following parameters in the contrast behavior of SWNTs was studied:

1. Primary electron landing energy, substrate conductivity, and imaging history

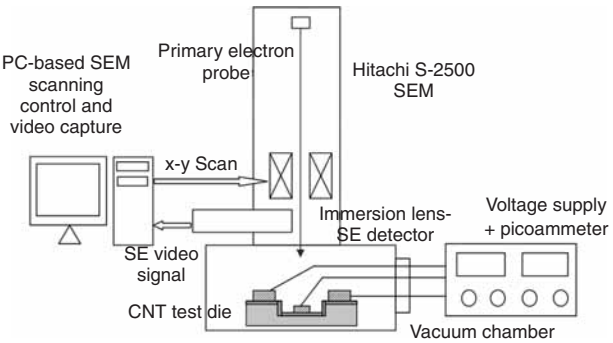

FIG. 4 In-situ single-walled carbon nanotube characterization experiment. PC = personal computer, SEM = scanning electron microscope, SE = secondary electron, CNT = carbon nanotube.

2. SWNT-substrate geometry and electron beam-induced contamination
3. Electrical biasing.

Results and Discussion

Secondary Electron Contrast of Single-Walled Carbon Nanotubes as a Function of Primary Electron Landing Energy, Substrate Conductivity, Electron Beam-Induced Contamination, and Imaging History.

One of the questions in the SEM of SWNTs is the extent of contrast contribution from the SWNT compared with the underlying substrate due to the limited degree of electron scattering in SWNTs. This property was previously investigated in the context of suspended CNTs in the transmission electron microscope (TEM) (Qin *et al.* 2001). Here, the behavior of SE emission from nonsuspended SWNTs in the presence of a 400 nm thick SiO_2 substrate was investigated; SiO_2 was chosen given the established use of Si-oxynitride dielectrics, as well as SiO_2's well-understood electron emission and electron beam-interaction properties such as the total electron yield unity crossover point (3.0 keV predicted using Monte Carlo simulations) (Joy 1989). Samples were imaged at a range of primary beam energies from 500 eV to 20 keV. In this part we focus on those nanotubes lying on the oxide surface, as opposed to the ones suspended across the trench. The SWNTs were floated electrically to allow for intrinsic charging (Fig. 5), as is the case in normal SEM imaging. The beam current of the SEMs was kept as low as possible (in the 1–3 pA range) and scanning performed predominantly at TV rates at moderately low magnifications (below 12,000×) in a vacuum of 1×10^{-5} Torr or better to limit electron beam-induced hydrocarbon contamination buildup on the SWNTs (more detail given in the following section). As will be discussed in the following sections, the resultant SE contrast was found to be independent of extrinsic parameters for suspended SWNTs and would remain bright consistently. Secondary electron contrast from nonsuspended SWNTs exhibited a dependence on contamination, substrate conductivity/charging, and electron beam-induced conductivity (EBIC) effects (i.e., extrinsically determined). For the device previously shown (Fig. 3) at a 500 eV primary energy (Fig. 5a), the total electron yield from the surrounding bulk SiO_2 is slightly higher than unity and the oxide therefore gains a small positive potential which does not interfere with nanotube imaging. The nanotubes thus show a normal strong bright contrast. This is not surprising since the SE yield from carbon is close to its maximum at a 500 eV primary energy (Reimer 1993). This bright contrast gradually decreases with primary energy until, at about 1.6 keV (see the nanotubes around the electrodes on Fig. 5(b), the nanotubes start to become invisible and eventually switch contrast and show a slightly dark contrast compared with the oxide. As the primary beam energy is increased further, the dark contrast becomes stronger up to a primary energy of 2.5 keV (Fig. 5c) shows a 2.0 keV case—note that compared with Fig. 3, which also shows an image at 2.0 keV, the nanotube contrast has changed from bright to dark). Beyond 2.5 keV, the dark contrast gradually decreases (see Fig. 5d for 3.5 keV) until, at a 4.8 keV primary energy, the nanotubes are almost invisible (Fig. 5(e). Then the contrast is reversed again, and nanotubes are bright compared with the oxide at higher primary beam energies (Fig. 5f for 10.0 keV), although not as bright as with low primary energies such as 500 eV.

We explain this behavior as follows: If the sample is being imaged at 2.0 keV for the first time (Fig. 3), not much charging and electron beam contamination have taken place; the nanotubes thus exhibit their normal bright contrast. Then, the primary energy is swept over a large range; first at 500 eV (Fig. 5a), the nanotubes again show bright contrast. Note that the oxide gradually gains positive charge at this primary energy (since it is below the unity yield crossover point of 3.0 keV for the oxide). As more and more images are taken of the sample, more and more charge accumulates in the oxide; this creates a positive potential on the oxide surface. Although the nanotubes might also gain some charge as a result of imaging, since they are connected to large metal electrodes (with a large capacitance), the charge that is left on them during this process will not change their potential significantly with respect to the substrate ($V = Q/C$ – large C results in small V). Furthermore, the electrodes are connected to large pads (several hundreds of microns across—not in the field of view in the figures) that, in addition to making the associated capacitance very large, help redistribute some of the nanotube charge. As a result, a potential difference and therefore electric field builds up between the nanotubes and the underlying oxide. This field will retard or "capture" a high number of the SEs emitted from the nanotube as well as from the oxide regions immediately adjacent to them, reducing the brightness in these regions (this effect is in principle similar to the characteristic dark "halo" around a dust particle when imaged in the SEM—in fact, a similar artifact can be seen around the edges of the electrodes in Fig. 5c and d). Therefore, the nanotubes lose their brightness with each captured image in this primary energy range, until they become almost invisible

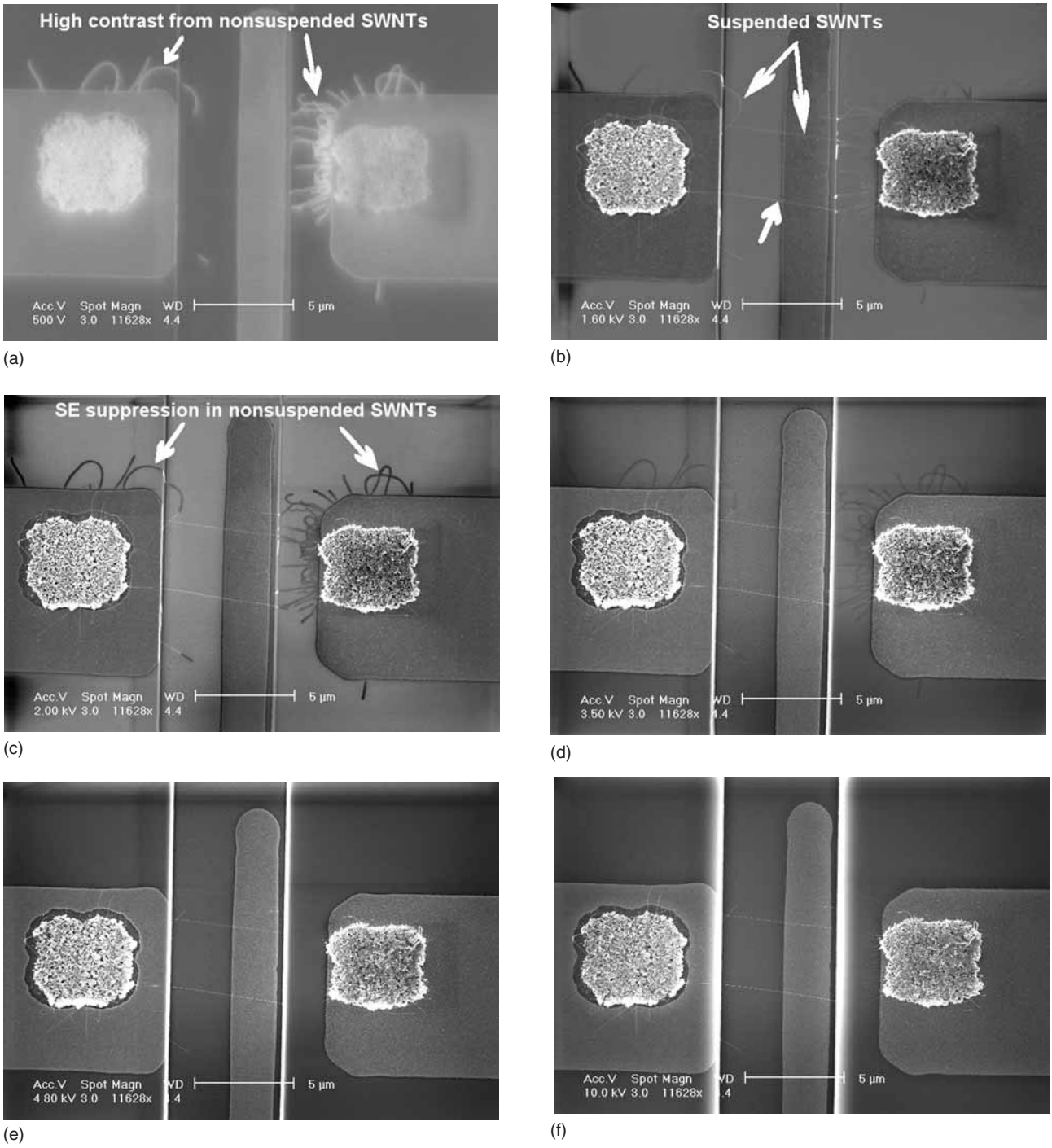

FIG. 5 Scanning electron micrographs of single-walled carbon nanotubes (SWNTs) in the order of imaging at (a) 500 eV; (b) 1.6 keV; (c) 2.0 keV; (d) 3.5 keV; (e) 4.8 keV; (f) 10.0 keV (horizontal field width = 25 µm, FEI Sirion SEM).

and then switch contrast: Figure 5c shows an image at 2.0 keV, where nanotubes are dark (note that when the sample was imaged for the first time at 2.0 keV [Fig. 3], the same nanotubes were bright). The dark SWNT contrast can in addition be attributed to suppressed SE emission from electron beam-induced contamination on the nonsuspended SWNTs, although this contamination buildup was limited by careful control of the electron-beam scan rate, magnification, and probe currents as discussed in greater detail in the following section. Figure 6 shows the morphology of this contamination layer via TEM analysis of an MWNT that had been inspected earlier in an SEM. This trend continues and the nanotubes become increasingly darker with each subsequent higher keV scan, until they arrive somewhere between 2.5 and 3.0 keV. Above

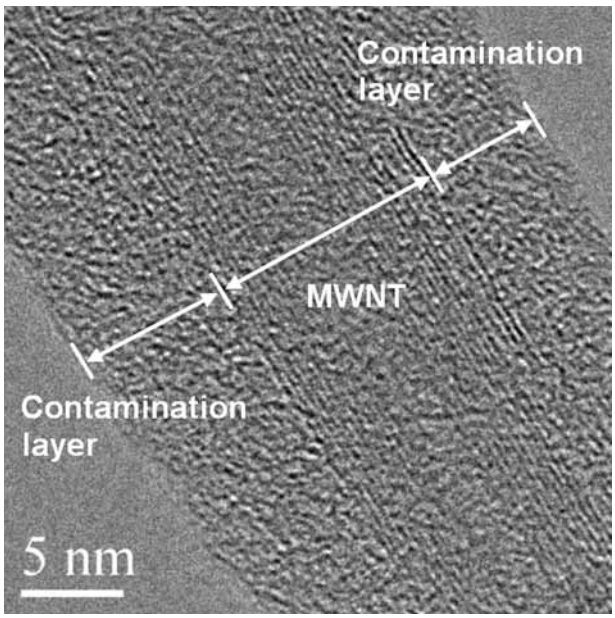

FIG. 6 Transmission electron microscopy analysis of electron beam (SEM) induced amorphous contamination layer on a multiwalled carbon nanotube (horizontal field width = 30 nm, JEOL JEM-2010F TEM).

3.0 keV, the total electron yield from the oxide is less than unity, and imaging creates negative charge in the oxide (Joy 1989). This negative charge gradually compensates the positive charge already existing in the oxide, and therefore the retarding field between the nanotubes and the oxide gradually decreases with each scan. Thus, the nanotubes gradually lose their dark contrast (Fig. 5d). Also, the general negative charging of the oxide surface everywhere makes the oxide surface darker, and this makes the dark contrast on the nanotubes increasingly less visible. This trend continues for primary beam energies up to about 4.8 keV (Fig. 5e), where EBIC kicks in, creating a transient conductive path through the ~400 nm thick SiO_2 (the theoretical Kanaya-Okayama electron range [Kanaya and Okayama 1972] for SiO_2 is approximately 400 nm at 4.5 keV). Therefore, the oxide now behaves as a noncharging substrate during primary electron irradiation. Without substrate charging, we observed intrinsic contrast behavior from the nonsuspended nanotubes on this sample at primary energies of 5 keV and above (Fig. 5f), similar to suspended nanotubes.

In next phase of the experiment, we increased the primary energy up to 18 keV and then decreased it again in steps. On the way back, the nanotubes again showed a bright contrast down to about a 5 keV primary energy, as before (Fig. 5f). After that (i.e., at primary energies <4.5 keV), the EBIC mechanism no longer exists and negative charge starts accumulating on the oxide. Going down in primary energies, this negative charging at each step between the EBIC point and the electron yield unity crossover point (approximately the 5–3 keV range) causes a stronger negative potential than on the way up, since now it is against an uncharged oxide background as opposed to a positively charged oxide. Thus, at each of these primary energies, the dark contrast of the nanotubes is stronger than at the same primary energy on the way up (Fig. 7). In the extreme cases of 3.0 keV (Fig. 7b) and 2.0 keV (Fig. 7c), even though the contrast is still dark as before, nanotubes appear much thicker and the image has halos and glows that suggest strong charging artifacts (compare Fig. 7c with Fig. 5c for the 2.0 keV case). One possible explanation for these enlarged SWNT shank diameters could be based on surface EBIC as the electron beam is scanning around the SWNT: the effective equipotential space is determined by the convolution of the SWNT shank and the EBIC radius at the oxide surface (e.g., the SWNT diameters in Fig. 7c are about 400 nm, which is about four times (i.e., twice the diameter) the Kanaya-Okayama electron range of 107 nm at 2.0 keV). However, this artifact correlates only with strong negative oxide charging (Figs. 7b–d). This could be because, in the presence of significant negative oxide charging, the effective landing energy of the primary electrons is retarded such that the penetration depth is very small and the electrons scatter in a roughly hemispherical interaction profile where surface EBIC plays a significant role. This electron scattering phenomenon has been studied thoroughly previously using Monte Carlo modeling (Goldstein et *al*. 1992). For the upsweep cases where there is much less negative charging (and hence not much retarding field for the primaries), the electron interaction profile has its normal pear/teardrop shape, where there is no significant lateral EBIC at the surface and hence there is no pronounced SWNT shank enlargement (this mechanism applies also to high-beam landing energies, i.e., >5 keV). The appearance of some of the halos in Figure 7c is reminiscent of those obtained due to electrons being reflected from a strongly negative-charged oxide surface, bouncing off of the pole piece and creating an image that is superimposed on the sample image, that is, the electrostatic mirror image microscopy mechanism (Vigouroux *et al*. 1985). Moreover, in cases similar to Figure 7c, if the sample is taken to air after the experiment for some time (to discharge any accumulated sample charging) and then put back in the SEM, the halos disappear and normal SE contrast is reinstated. This is another reason to believe that the artifacts shown in Figure 7 are primarily due to negative charging of the oxide and not a permanent effect such as contamination. It is surprising that, at 1.0 keV (Fig. 7d), the contrast is still dark, which is the opposite of what was observed in the previous half of the experiment, when the primary energy was being increased. This is because the positive charging of the oxide while imaging at 2.0 and 1.0 keV has not been enough to compensate the negative charge already present from imaging at higher primary energies (Wong *et al*. 1997). This effect may be thought of as a hysteresis phenomenon. However, at 500 eV, the nanotubes become bright again (Fig. 7e) and the image is similar to the first captured image (Fig. 5a), except for a slightly darker contrast from the oxide due to residual negative charge. From these results, we believe that the interaction of the primaries with the nanotube is quite different from the multiple scatterings that happen in bulk samples. In fact, the lower the primary

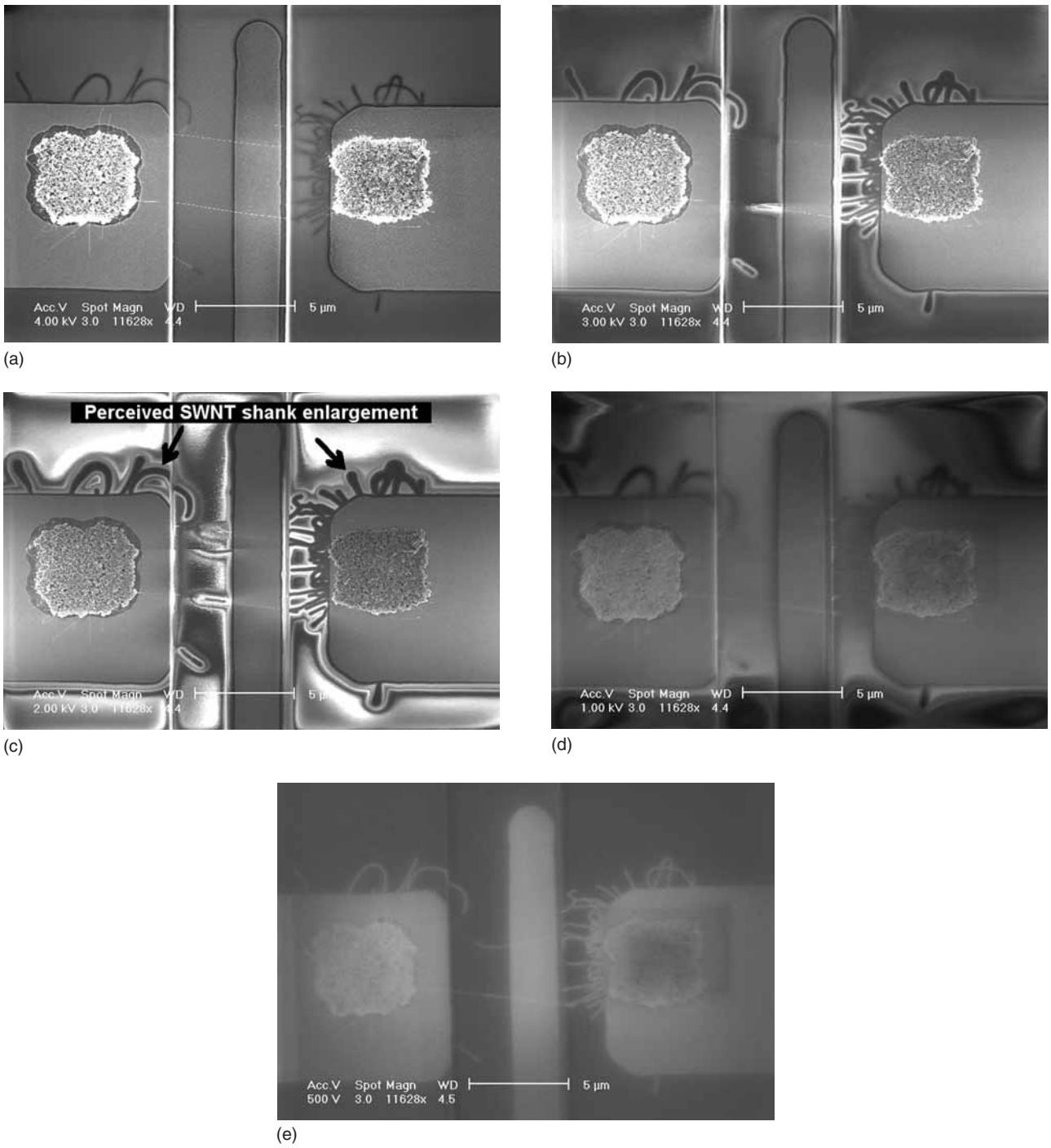

FIG. 7 Scanning electron micrographs of single-walled carbon nanotubes in the order of imaging at (a) 4.0 keV; (b) 3.0 keV; (c) 2.0 keV; (d) 1.0 keV; (e) 500 eV (horizontal field width = 25 µm, FEI Sirion SEM).

energy, the more time the primaries spend inside the nanotube, and the stronger the interaction. The negative oxide surface potential retards the 500 eV primaries to very low velocities and enhances their interaction with the nanotubes, thus creating such bright nanotube images. Going back up to 2 keV creates an image like in Figure 7c again, with all the glows and halos since a residual negative charge is still present in the oxide. The above-mentioned behavior of nonsuspended SWNTs is further corroborated by the high SE contrast observed in suspended SWNTs (discussed in the next section) independent of the primary beam energy, and highlights the limitation of beam–bulk interaction models, which predict minimal scattering and hence very low SE yields from SWNTs. More comprehensive models would need to consider quantum

mechanical interaction physics in order to account for the significant SWNT SE contrast, particularly at low beam-landing energies (Nojeh *et al*. 2006).

Role of Single-Walled Nanotube-Substrate Geometry, Electron Dose and Contamination

For suspended SWNTs, the contrast derived from the SWNT is mainly from the direct interaction between the primary electron beam and the SWNT itself, compared with the substrate dependency for nonsuspended SWNTs. As can be seen in Figure 5a–f, the contrast behavior of the suspended SWNTs over the trench is independent of beam-landing energies, with a stable SE contrast observed over the entire range. The separation of the SWNT from the substrate plays a critical role in the imaging process. Figure 8 illustrates this effect where reduced SE emission is observed for the sections of SWNTs that are in contact with the substrate, with contact being ascertained by imaging the samples at an angle (not shown). This shows that the intrinsic SE contrast of the SWNTs is observed in the case of suspended SWNTs, compared with the electron beam energy and substrate charging dependence for nonsuspended SWNTs discussed in the previous section.

Another reason for the contrast difference between suspended and nonsuspended sections relates to the dynamics of electron beam-induced contamination buildup on sample surfaces, where carboneous contamination builds up at a higher rate on the nonsuspended sections of SWNTs due to surface diffusion of hydrocarbons present on the sample surface; direct adsorption from the vacuum has been found to be a relatively insignificant contamination mechanism (Amman *et al*. 1996). The net result would be a thicker contamination buildup for the nonsuspended compared with the suspended sections of the SWNT, resulting in lower SE yield from the nonsuspended sections. Figure 6 shows a TEM cross-section of this contamination buildup.

Figure 9 shows the SE contrast characteristics of SWNTs at 1.5 keV after a layer of contamination was deposited on the sample by slow scan exposures of approximately 100 and 500 $\mu C/cm^2$ using a 10 keV primary electron beam in the Hitachi S-2500 SEM. The vacuum pressure was in the 5×10^{-5} Torr range. The contrast of the amorphous carbon contamination, particularly on the nonsuspended SWNTs was found to dominate in this case as evidenced by the reduced SE contrast of the SWNTs, lying on the oxide surface within the primary exposure zones. We found this effect to be particularly pronounced for postcontamination inspection at lower (<4 keV) beam energies. Conversely, the electron exposures have negligible influence on the SE contrast of suspended SWNTs across the trench, thus providing further evidence of surface diffusion-dominated contamination.

Note that for the experiments discussed in the previous section (Figs. 5 and 7), given the better vacuum conditions of the FEI Sirion microscope (FEI Company, Hillsboro, OR, USA) compared with the Hitachi S-2500 (about 5 to 10 times better), a generally higher level of irradiation than the above-mentioned 100 $\mu C/cm^2$ would be needed to build enough contamination to affect the nanotube contrast. At an average probe current of about 2 pA, a 25×20 μm scan field, and single-frame capture times of 30 s at slow

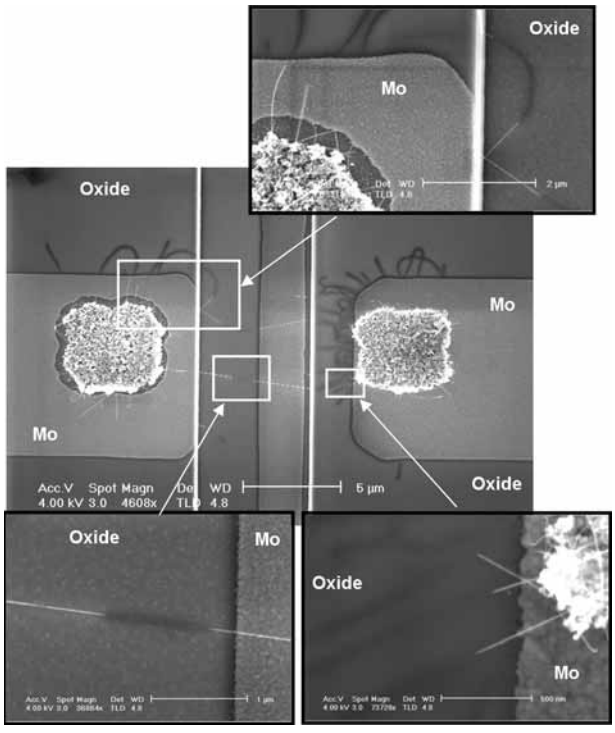

FIG. 8 Variations in secondary electron contrast at 4.0 keV for single-walled carbon nanotubes in partial contact with SiO_2 (insulating) and molybdenum (conducting) substrates (various horizontal field widths from 1.7–27 μm, FEI Sirion SEM).

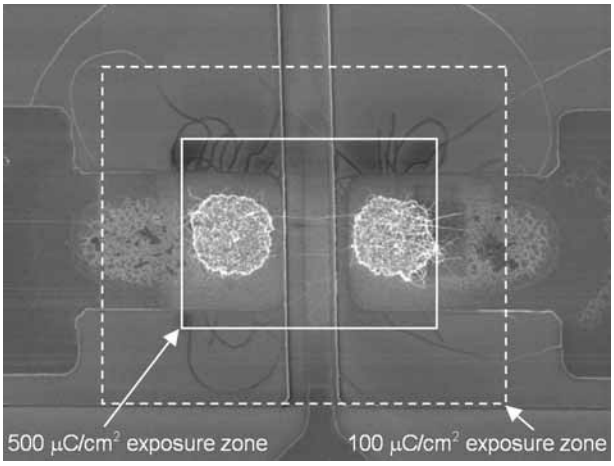

FIG. 9 Effect of electron beam-induced amorphous hydrocarbon contamination on single-walled carbon nanotube contrast (1.5 keV micrograph, horizontal field width = 42 μm, Hitachi S-2500 SEM).

scan, we have single-frame electron dose values of about 10 μC/cm^2. Therefore, we can safely assume that the results shown in Figures 5 and 7 were not dominated by contamination buildup. However, it is important to emphasize that the contamination history is an important parameter and hence should always be taken into account when interpreting slow scan SEM images of SWNTs under nonultra high vacuum (UHV) conditions (above 10^{-8} Torr).

From the above-mentioned discussions, we can conclude at this juncture that SEM image contrast of SWNTs is a complex aggregate of the their direct interaction with the electron beam as well as extrinsic factors such as sample-substrate geometry, substrate charging, contamination, effective electron-beam landing energy, and the sample's imaging history. Observations such as SWNT diameter variations across the full range (500 eV–30 keV) of primary beam energies are not fully explained by sample potential (Brintlinger *et al*. 2002) and substrate EBIC effects (Homma *et al*. 2004). More work is in progress on modeling the SE emission process from nanotubes using ab initio quantum calculations.

Inspection of Single-Walled Carbon Nanotubes in the Scanning Electron Microscope under in-situ Electrical Biasing.

Electrical bias can alter the emission behavior of nonsuspended SWNTs such that consistent sample contrast is achieved irrespective of contamination and substrate charging effects, especially at low-beam inspection energies. In the present experiment, the primary electron energy was swept from 2.0 to 25 keV. At each beam energy, a bias range of −50 to 50 V was applied to the SWNTs concurrently with SEM imaging. It was observed that the SE contrast of the SWNTs can be radically changed across the entire range of beam energies using voltage biasing. For example, a negative bias to the SWNT up to −20V, as shown in Figure 10, can be used to overcome the SE suppression and gross shank distortion artifacts at low primary beam energies. This result concurs with those by Brintlinger *et al*. (2002), in which the SWNT contrast mechanism was suggested to depend on the electrical potential of the SWNT and not on the direct backscattering of the electron beam by the SWNT. Conversely, SWNT SE emission can also be suppressed using positive bias voltages (not shown). Hence, in-situ SWNT electrical biasing can be used to remove the primary beam energy dependence of CNT SE contrast and to customize the CNT contrast depending on analysis requirements. One advantageous operating point would be to use low-beam energies to 1) maximize primary electron interaction and hence SE signal contribution from the SWNT relative to the substrate; 2) reduce electron beam-induced contamination and damage to the SWNTs; and 3) achieve more accurate SWNT shank metrology by using negative biasing to overcome SE suppression artifacts.

Figure 11 summarizes the values of SWNT bias voltage thresholds required to achieve SE contrast reversal for a SWNT on a 400 nm thick SiO_2 substrate. Of particular note is the x-axis intersection at around 4.5 keV, which is determined by the onset of EBIC conduction through the 400 nm thick oxide.

However, a limit exists for SWNT negative biasing due to the occurrence of electron field-emission in SWNTs because of pronounced electric field enhancement of the high SWNT aspect ratios (the maximum allowable bias value is sample dependent). Also, in some cases (depending on the nanotube chirality and tip structure—capped, open, passivated) at subthreshold bias levels for normal (spontaneous) electron emission, the presence of an external stimulus, for example, an electron from the primary beam, can provide the trigger for electron emission. Therefore, emission happens only when the primary beam strikes the nanotube tip, resulting in bright spots (Fig. 12). We call this stimulated field emission (SFE) (Nojeh *et al*. 2004). As the duration of the SFE events can last up to 1 ms, bright streaks in the x direction corresponding to the direction of the raster scan appear in the resultant slow-scan SEM image as shown in Figure 12.

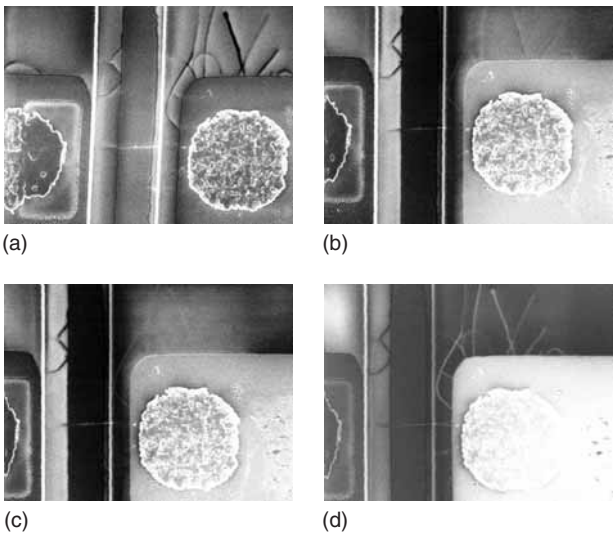

FIG. 10 Micrographs showing the effect of single-walled carbon nanotube voltage bias at 3.0 keV: (a) 0V (no bias); (b) -8.0V; (c) −8.8V; (d) −20V (horizontal field width = 12 μm, Hitachi S-2500 SEM).

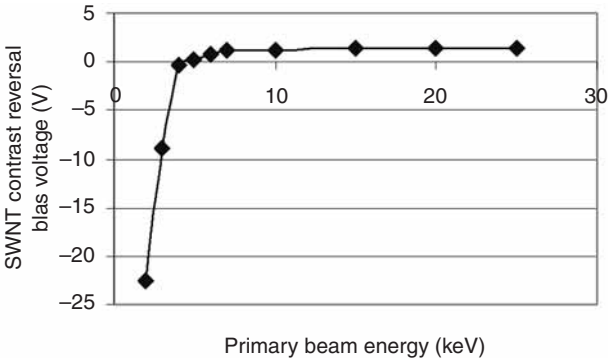

FIG. 11 Bias voltage thresholds for nanotube contrast reversal as a function of primary electron landing energy. SWNT = single-walled carbon nanotube.

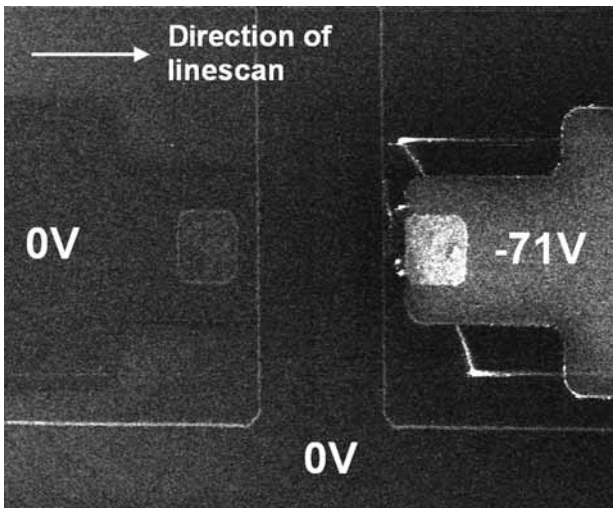

FIG. 12 Stimulated field emission (SFE) in single-walled carbon nanotubes biased at −71V observed in the scanning electron microscope at 3.0 keV (horizontal field width = 45 μm, Hitachi S-2500 SEM) (Nojeh et al. 2004).

Conclusion

The contrast characteristics, including contrast reversal, of SEM images of SWNTs depend strongly on many factors, including primary beam-landing energy, history of imaging, whether the SWNT is lying on a substrate or is suspended, substrate electrical conductivity and electron beam-induced contamination. Hence, these factors need to be taken into account when interpreting such images. Voltage biasing of the SWNT can modify SE emission from SWNTs and their immediate surroundings. Also, for a SWNT lying on a substrate, higher SE emission from the SWNT than from an insulating substrate generally yields a more accurate representation of the width of the SWNT. However, SWNT shank diameters observed in SEM images are larger than those from AFM images and both exceed theoretical values. Ab initio theoretical modeling is underway for further study of electron beam-specimen interaction physics in SWNTs and a better explanation of the SEM image contrast characteristics of these samples.

Acknowledgments

The authors would like to thank Professor Hongjie Dai of the Stanford Chemistry Department for his help in preparing the samples and Eric Yieh for assisting in the preparation of the experimental apparatus. Fabrication was performed in part at the Stanford Nanofabrication Facility of NNIN supported by National Science Foundation under Grant ECS-9731293. The additional contributions of Lei Wang and Soon-huat Lim at the National University of Singapore to the research work are also acknowledged.

References

Amman M, Sleight JW, Lombardi DR, Welser RE, Deshpande MR, Reed MA, Guido LJ: Atomic force microscopy study of electron beam written contamination structures. *J Vac Sci Technol B* 14, 1, 54–62 (1996)

Brintlinger T, Chen YF, Durkop T, Corbas E, Fuhrer MS: Rapid imaging of nanotubes on insulating substrates. *Appl Phys Lett* 81, 13, 2454–2456 (2002)

Cassell A, Raymakers J, Kong J, Dai H: Large scale CVD synthesis of single-walled carbon nanotubes *J Phys Chem B* 103, 6484–6492 (1999)

Goldstein JI, Newbury DE, Echlin P, Joy DC, Romig AD Jr., Lyman CE, Fiori C, Lifshin E: *Scanning Electron Microscopy and X-Ray Microanalysis*. Plenum Press, New York (1992) 79–87

Homma Y, Suzuki S, Kobayashi Y, Nagase M: Mechanism of bright selective imaging of single-walled nanotubes on insulators by scanning electron microscopy. *Appl Phys Lett* 84, 10, 1750–1752 (2004)

Iijima S: Helical microtubules of graphitic carbon. *Nature* 354, 56–58 (1991)

Joy DC: Control of charging in low-voltage SEM. *Scanning* 11, 1–4 (1989)

Kanaya K, Okayama S: Penetration and energy-loss theory of electrons in solid targets. *J Phys D* 5, 1, 43–58 (1972)

Martel R, Schmidt T, Shea HR, Hertel T, Avouris P: Single- and multi-wall carbon nanotube field-effect transistors. *Appl Phys Lett* 73, 17, 2447–2449 (1998)

Nojeh A, Wong WK, Yieh E, Pease RF, Dai HJ: Electron beam stimulated field-emission from single-walled carbon nanotubes. *J Vac Sci Technol B* 22, 6, 3124–3127 (2004)

Nojeh A, Shan B, Cho K, Pease RFW: *Ab initio* modeling of the interaction of electron beams and single-walled carbon nanotubes. *Phys Rev Lett* 96, 056802 Epub (2006)

Qin LC, Zhao X, Hirahara K, Ando Y, Iijima S: Electron microscopic imaging and contrast of smallest carbon nanotubes. *Chem Phys Lett* 349, 389–393 (2001)

Radosavljevic M, Freitag M, Thadani KV, Johnson AT: Nonvolatile molecular memory elements based on ambipolar nanotube field effect transistors. *Nano Lett* 2, 7, 761–764 (2002)

Reimer L: *Image Formation in Low-Voltage Scanning Electron Microscopy*. SPIE Optical Engineering Press, Bellingham, Washington (1993) 57–78

Vigouroux JP, Duraud JP, LeMoel A, LeGressus C: Electron trapping in amorphous SiO_2 studied by charge buildup under electron bombardment. *J App Phys* 57, 12, 5139–5143 (1985)

Wong WK, Phang JCH, Thong JTL: A novel method for the discharge of electrostatic mirror formations in the scanning electron microscope. *Scanning* 19, 498–504 (1997)